

THESIS FOR THE DEGREE OF LICENTIATE OF ENGINEERING

LOWER HYBRID CURRENT DRIVE IN THE
TORE SUPRA TOKAMAK

Emelie Nilsson



CHALMERS

Department of Applied Physics
Chalmers University of Technology
Göteborg, Sweden, 2014

LOWER HYBRID CURRENT DRIVE IN THE TORE SUPRA TOKAMAK
Emelie Nilsson

© Emelie Nilsson, 2014

Technical Report No. CTH-NT-303
ISSN 1653-4662
Nuclear Engineering
Department of Applied Physics
Chalmers University of Technology
SE-412 96 Göteborg
Sweden
Telephone +46-(0)31-772 10 00

This work has been carried out in collaboration with CEA/IRFM,
F-13108, Saint-Paul-lez-Durance, France.

Some figures in this thesis are in color only in the electronic version,
available online through Chalmers Publication Library.

The image illustrates the poloidal projection of the propagation of one
of the rays in the lower hybrid wave in the Tore Supra tokamak,
modelled with ray-tracing/Fokker-Planck codes.
See p. [32](#) for more details.

Printed in Sweden by
Reproservice
Chalmers Tekniska Högskola
Göteborg, Sweden, 2014

Abstract

To control and extract energy from nuclear fusion reactions, a mixture of deuterium and tritium gases must be heated to temperatures on the order of 100 million degrees, whilst maintaining a sufficiently high density. The main difficulty is to confine the ionised gases, i.e. plasma, until the rate of fusion reactions becomes large enough. In the most promising type of magnetic confinement fusion device, known as tokamak, steady state operation is highly desirable and can only be reached by non-inductive current drive methods, to complement the confining magnetic field. The best, experimentally proven method is by injection of lower hybrid (LH) waves that transfer momentum to the electrons in the plasma.

In the Tore Supra tokamak, LH waves at a frequency of 3.7 GHz are coupled to the plasma for current drive using a fully active multijunction (FAM) launcher and/or a passive active multijunction (PAM) launcher, which was installed recently to test an antenna design relevant for ITER, which is the next large-scale tokamak currently under construction. In this thesis a study of fully non-inductive discharges with either the FAM or PAM launchers is performed, using a suite of codes specifically developed for LH current drive. Good agreement is found between experiments and simulations for such discharges at relatively low density. A detailed comparison of the LH power deposition profile and current drive efficiency with the two launchers is made. The parallel refractive index spectra (n_{\parallel}) of the two launchers are found to be noticeably different, resulting in different current profiles.

Keywords: fusion plasma physics, tokamak, lower hybrid current drive, radio frequency waves, launcher, fast electron dynamics

Publications

- [A] E. Nilsson, J. Decker, Y. Peysson, J.-F. Artaud, A. Ekedahl, J. Hillairet, T. Aniel, V. Basiuk, M. Goniche, F. Imbeaux, D. Mazon and P. Sharma.
Comparative modelling of lower hybrid current drive with two launcher designs in the Tore Supra tokamak.
Nuclear Fusion **53**, 083018 (2013).
<http://stacks.iop.org/0029-5515/53/i=8/a=083018>.
- [B] M. Goniche, V. Basiuk, J. Decker, P.K. Sharma, G. Antar, G. Bergerby, F. Clairet, L. Delpech, A. Ekedahl, J. Gunn, J. Hillairet, X. Litaudon, D. Mazon, E. Nilsson, T. Oosako, Y. Peysson, M. Preynas, M. Prou and J.L. Segui.
Lower hybrid current drive at high density on Tore Supra.
Nuclear Fusion **53**, 033010 (2013).
<http://stacks.iop.org/0029-5515/53/i=3/a=033010>.
- [C] J. Decker, Y. Peysson, J.-F. Artaud, E. Nilsson, A. Ekedahl, M. Goniche, J. Hillairet and D. Mazon.
Damping of lower hybrid waves in large spectral gap configurations. *Physics of Plasmas* **21**, 092504 (2014).
<http://scitation.aip.org/content/aip/journal/pop/21/9/10.1063/1.4894749>.

Futher publications (not included in the thesis)

- [D] E. Nilsson, J. Decker, Y. Peysson, J.-F. Artaud, A. Ekedahl, J. Hillairet, T. Aniel, M. Goniche, T. Hoang, F. Imbeaux, D. Mazon and P.K. Scharma.
Comparative modelling of LHCD with Passive-Active and Fully-Active Multijunction launchers in Tore Supra tokamak.
In *Europhysics Conference Abstracts*, volume 36F, P2.081, Stockholm, Sweden (2012).
<http://ocs.ciemat.es/EPSICPP2012PAP/pdf/P2.081.pdf>
- [E] J. Hillairet, A. Ekedahl, M. Goniche, Y.S. Bae, J. Achard, A. Armitano, B. Beckett, J. Belo, G. Berger-By, J.M. Bernard, E. Corbel, L. Delpech, J. Decker, R. Dumont, D. Guilhem, G.T. Hoang, F. Kazarian, H.J. Kim, X. Litaudon, R. Magne, L. Marfisi, P. Mollard, W. Namkung, E. Nilsson, S. Park, Y. Peysson, M. Preynas, P.K. Sharma and M. Prou.
Recent progress on lower hybrid current drive and implications for ITER. *Nuclear Fusion* **53**, 073004 (2013).
<http://stacks.iop.org/0029-5515/53/i=7/a=073004>.
- [F] R. Dumont, M. Goniche, A. Ekedahl, B. Saoutic, J.-F. Artaud, V. Basiuk, C. Bourdelle, Y. Corre, J. Decker, D. Elbéze, G. Giruzzi, G.T. Hoang, F. Imbeaux, E. Joffrin, X. Litaudon, Ph. Lotte, P. Maget, D. Mazon and E. Nilsson.
Multi-megawatt, gigajoule plasma operation in Tore Supra.
Plasma Physics and Controlled Fusion **56**, 075020 (2014).
<http://iopscience.iop.org/0741-3335/56/7/075020>.
- [G] J. Decker, E. Nilsson, Y. Peysson, J.-F. Artaud, A. Ekedahl, J. Hillairet, T. Aniel, M. Goniche, T. Hoang, F. Imbeaux, D. Mazon and P.K. Sharma.
Modelling of LHCD at various densities in Tore Supra tokamak.
In *Europhysics Conference Abstracts*, volume 36F, P2.094, Stockholm, Sweden (2012).
<http://ocs.ciemat.es/EPSICPP2012PAP/pdf/P2.094.pdf>

- [H] R.J. Dumont, M. Goniche, J.-F. Artaud, V. Basiuk, C. Bourdelle, Y. Corre, J. Decker, A. Ekedahl, D. Elbéze, G. Giruzzi, G.-T. Hoang, F. Imbeaux, X. Litaudon, Ph. Lotte, P. Maget, D. Mazon, E. Nilsson and B. Saoutic.
Advances in multi-megawatt, long pulse operation in Tore Supra. In *Europhysics Conference Abstracts*, volume 36F, P4.005, Stockholm, Sweden (2012).
<http://ocs.ciemat.es/EPSICPP2012PAP/pdf/P4.005.pdf>.
- [I] B.J. Ding, J. Decker, A. Ekedahl, P. Lotte, P. Maget, E. Nilsson, Y. Peysson, T. Aniel, J.-F. Artaud, V. Basiuk, R. Dumont, M. Goniche, J. Hillairet, F. Imbeaux and D. Mazon.
Effect of launched LH wave spectrum on current profile and MHD activity in Tore Supra. In *Europhysics Conference Abstracts*, volume 37D, P4.185, Espoo, Finland (2013).
<http://ocs.ciemat.es/EPS2013PAP/pdf/P4.185.pdf>.

Contents

Abstract	iii
Publications	v
Acknowledgements	xi
Abbreviations	xiii
1 Introduction	1
2 Magnetized fusion plasmas	5
2.1 Plasma confinement	7
2.2 Toroidal plasma current	9
2.3 Current drive methods	10
3 Lower Hybrid Current Drive	13
3.1 Landau damping	17
3.2 Kinetic description	17
3.3 Spectral properties of launched wave	20
4 Modelling of LHCD for Tore Supra plasmas	23
4.1 The LHCD system in Tore Supra	24
4.2 LHCD modelling	27
4.2.1 Core plasma modelling (METIS)	27
4.2.2 LH wave coupling (ALOHA)	28
4.2.3 Ray-tracing/Fokker-Planck (C3PO/LUKE)	32
4.2.4 FEB reconstruction (R5X2)	33
4.2.5 Summary of LHCD modelling	35
5 Summary	37

References	41
Included papers A–C	45

Acknowledgments

I would like to thank Tünde Fülöp, who introduced me to fusion physics and did not give up on me despite my temporary drift towards astro- and particle physics. Your dedication to science and your students is impressive and a great inspiration.

This work has been carried out at the CEA research center in Cadarache in southern France. I would like to thank the IRFM (Institut de Recherche sur la Fusion par confinement Magnétique) institute for the unique opportunity to work with world leading scientists on cutting edge nuclear fusion research. I thank the Tore Supra team for the fruitful work and making me feel at home in France. Deepest gratitude to my supervisor Annika Ekedahl for her invaluable guidance and expertise in the lower hybrid current drive physics. Thank you for supporting me from day one. My greatest appreciation to the enthusiastic supervision from Joan Decker, for his encouragement and creative mind. Yves Peysson, expert of LHCD and alpinism: Thank you for all your good advice and support in the research as well as on the glacier.

Inspirations and colleagues in LH physics: Marc Goniche, Julien Hillairet, Xavier Litaudon, Jean-Francois Artaud, Melanie Preynas, Walid Helou, Gerardo Giruzzi, Nathaniel Fisch and Torbjörn Hellsten. Thanks for all the interesting discussions! Thanks to colleagues and friends who inspire me in work as well as in life: Claudia Norcini, Farah Hariri, Albert Mollén, Adam Stahl, Geri Papp, Istvan Pusztai, Jakob Ryden, Robert Nyqvist, Joel Rasch, Sarah Newton, Billal Chouli, Hugo Arnichand, Alexandre Fil and Jorge Morales. For the fun times, summer schools, conferences and trips we shared.

Finally I thank Philip, Lovisa and Adam. My dear sister and brothers who just began their studies this year. You can do it! Remember to have fun and stay curious.

Abbreviations

Acronyms

ALOHA	A dvanced L ower H ybrid A ntenna
FAM	F ully A ctive M ultijunction
FEB	F ast E lectron B remsstrahlung
FP	F okker- P lanck
HXR	H ard X - R ay
ICRH	I on C yclotron R esonance H eating
LCFS	L ast C losed F lux S urface
LHCD	L ower H ybrid C urrent D rive
METIS	M inute E MBEDDED T OKAMAK I ntegrated S imulator
MHD	M agneto H ydro D ynamic(s)
NBI	N eutral B eam I njections
PAM	P assive A ctive M ultijunction
RF	R adio F requency
SOL	S rape O ff L ayer

Magnetic confinement fusion devices

TS	T ore S upra, CEA, Cadarache, France
ITER	“ T he W ay” in Latin Under construction in Cadarache, France
LHD	L arge H elical D evice, National Institute for Fusion Studies, Nagoya, Japan
PLT	P rin C eton L arge T orus, Princeton University, Princeton NJ, USA
WEST	T ungsten (W) E nvironment in S tady-state T okamak Upgrade from Tore Supra in Cadarache, France

Chapter 1

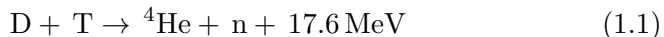
Introduction

Increasing global energy demand driven by population growth and rising standards of living is causing environmental problems on Earth. The main energy sources of today are limited and give rise to the greenhouse effect and pollution. To meet the energy needs of a growing global population, sustainable energy production with much lower environmental impact than conventional technologies must be developed.

Controlled nuclear fusion has some very valuable properties as an energy source. It can be made inherently safe and fuel resources are well accessible all over the planet. With no direct contribution to the greenhouse effect and absence of long duration waste that would burden future generations, fusion energy is an attractive candidate for delivering clean, reliable and virtually inexhaustible energy.

Though still a somewhat exotic topic on Earth, nuclear fusion is the main energy source of our universe. In the Sun and other stars, hydrogen nuclei fuse and release enormous amounts of energy. Confined by strong gravitational pressure, the Sun is a gigantic fusion reactor that sustains our existence on Earth. By combining light nuclei into heavier elements, energy is released through the difference in binding energy of nuclei according to the formula $E = mc^2$. The goal in fusion energy research is to recreate this process in a reactor on Earth.

There are several candidates for the fuel in a fusion reactor. The reaction between the hydrogen isotopes deuterium (^2H or D) and tritium (^3H or T) has by far the largest cross-section at the lowest energies (see Fig. 1.1) [1]. This makes the D-T fusion process



the most promising reaction for an energy producing system.

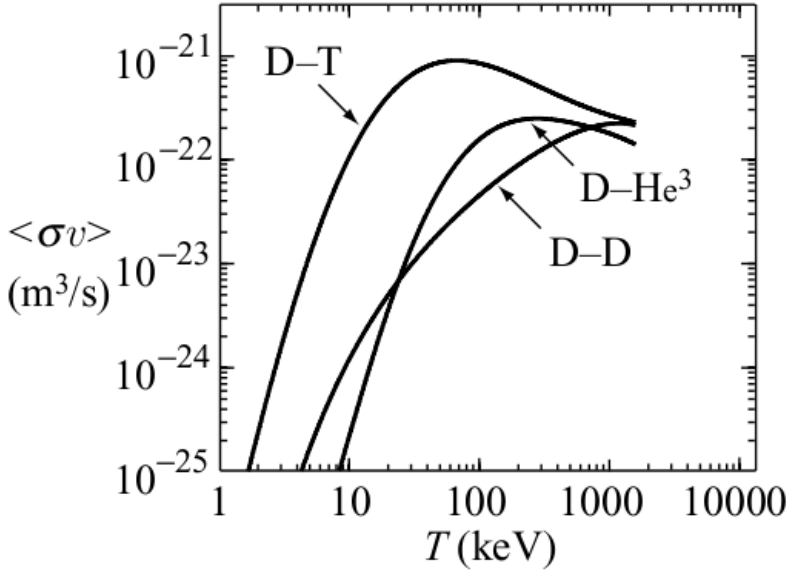
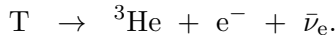
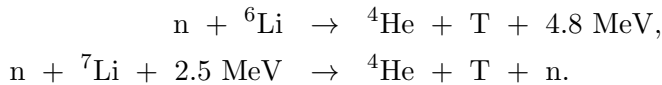


Figure 1.1: The velocity averaged cross section of fusion reactions as a function of temperature, obtained numerically from equal temperature Maxwellian distributions. The D-T reaction has a maximum reaction cross section at a temperature of around 70 keV. Adapted from [2].

In the pursuit of a sustainable energy producing system, the fusion fuel also has to be sufficiently abundant. Deuterium occurs naturally with a weight fraction of 3.3×10^{-5} in water. Thus the fuel is abundant and accessible worldwide and on a long term, given the water available in the oceans. Tritium is a radioactive isotope of hydrogen with a half-life of 12.3 years. It decays into ${}^3\text{He}$



Owing to its unstable character, no significant amount of tritium exists in nature, but it can be produced with nuclear reactions of the neutrons from the D-T reaction and lithium:



As two nuclei approach, they repel each other because of their positive charge. In order to fuse, they must be brought very close, to a

range on the order of 10^{-15} meters, where the attractive nuclear force is strong enough to overcome the electrostatic potential barrier. In the center of a star the enormous gravitational pressure provides the nuclei with enough energy to overcome the Coulomb repulsion and fuse. For the nuclei to overcome the electrostatic potential barrier they have to collide at very high speeds. This means that the temperature of the fuel has to be very high, on the order of 100 million degrees. At these temperatures, which are ten times higher than in the center of the Sun, the nuclei of the fuel are stripped from their electrons. This state of matter is called a *plasma* and is a mix of positively charged ions and free electrons. On Earth other confinement methods must be used to keep the fuel in plasma state long enough for a significant part of it to fuse. The charged particles in a plasma gyrate around magnetic field lines. This is the principle behind magnetic confinement fusion, where strong magnetic fields control the motion of the plasma particles through the Lorentz force.

The aim of fusion research is to create a so called burning plasma, in which the heating power released in fusion reactions keeps the plasma hot enough to require no external heating. A fireplace is a chemical example of ignition. One uses a match to heat the fuel and once the burning of the wood releases heat faster than the air can carry it away the fire ignites and keeps burning. In a fusion reactor, one wants to initially heat up the fuel, and then let it burn without much external power being added. Unfortunately, current fusion experiments are like wet wood fires: to keep the reaction going, external heat must constantly be added.

At this point we have succeeded in achieving fusion reactions, but it has proven difficult to confine the fuel well enough at high temperature to make nuclear fusion a practical source for electrical power [3]. Fusion research is therefore focused on confining heat inside the plasma so that the reactor can ignite. Recreating the controlled fusion process on Earth is a great scientific and technological challenge. Mastering the complex technology of a fusion reactor has an amazing reward: clean, safe and accessible energy that can meet the energy needs of a growing population.

One of the most researched types of magnetic confinement devices for controlled fusion is the tokamak. In such a device the magnetic field must be partly generated by non-inductive current drive methods in order to allow for steady-state operation. This thesis deals with current

drive through injection of lower hybrid waves in tokamak plasmas. The following chapters of this thesis give an introduction to the concept of lower hybrid current drive and background to the attached publications. An introduction to the general concept of tokamak plasmas is given in chapter 2, followed by chapter 3 where the lower hybrid current drive physics is presented. This work has been carried out at the research institute IRFM (Institut de Recherche sur la Fusion par confinement Magnétique) at CEA (Commissariat à l'énergie atomique et aux énergies alternatives) where Tore Supra, one of the largest superconducting tokamaks in the world, is situated. The lower hybrid current drive system of the Tore Supra tokamak is presented in chapter 4 along with modelling tools and diagnostics used for validation of the simulations with experiments. Finally, in chapter 5 the attached papers are summarised and their main results for lower hybrid current drive are put into perspective.

Chapter 2

Magnetized fusion plasmas

The aim of the present chapter is to introduce some fundamental concepts of toroidally shaped fusion plasmas. Since any material would melt in contact with the hot fuel needed for fusion reactions to occur, the plasma must be prevented from touching the walls of the confinement chamber. The most promising method is magnetic confinement fusion where the motion of charged particles of the plasma is constrained by strong magnetic fields. The two main magnetic confinement fusion concepts are the *tokamak* and the *stellarator*. Both devices confine the plasma in a torus shaped magnetic cage, where the magnetic field consists of toroidal and poloidal components (ϕ and θ in Fig. 2.1). The main difference between the two confinement concepts is that in a stellarator the magnetic field is created by complex shaped external coils, whereas the tokamak is axisymmetric and the poloidal magnetic field component is generated by a strong electric current flowing in the plasma.

One of the largest superconducting tokamaks in the world, Tore Supra (see Fig. 2.2), is situated at the nuclear research center of Cadarache in southern France where it operates since 1988 [4]. Thanks to the use of superconducting magnetic field coils, water cooled plasma facing components and a long-pulsed non-inductive current drive system, Tore Supra is an important device for studying the physics and technology related to long pulse tokamak operation. At the moment Tore Supra is being upgraded to a tokamak dedicated to the test of tungsten divertor concepts and to physics related to long pulse operation with tungsten plasma facing components. The so called WEST (Tungsten (W) Environment in Steady-state Tokamak) configuration will have its first plasma planned for the year 2016 [5].

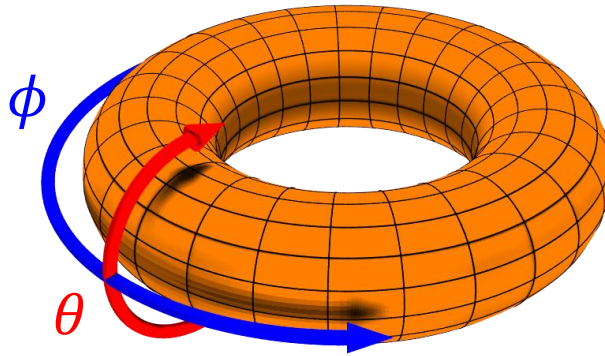


Figure 2.1: The toroidal (ϕ) and poloidal (θ) direction.



Figure 2.2: The Tore Supra tokamak.

2.1 Plasma confinement

A plasma consists mainly of free electrons, ions and neutrals. These charged particles can move freely along magnetic field lines, but their movement perpendicular to the field lines is restricted due to the Lorentz force ($\mathbf{F} = q\mathbf{v} \times \mathbf{B}$, where q is the charge of the particle, \mathbf{v} the particle velocity and \mathbf{B} the magnetic field) acting on charged particles, i.e. the positively charged nuclei and negatively charged electrons that form the plasma. The Lorentz force guides the particles to move perpendicularly to magnetic field lines in a circular motion resulting in gyrating particle orbits.

In a cylindrical magnetic confinement device the plasma particles would be confined perpendicularly to the field lines, but escape parallel to them at the ends of the cylinder. By bending the cylinder into a torus shaped device end losses can be eliminated.

The curvature of the toroidal field introduces forces on the plasma that cause particle drifts. The particles tend to drift away from the magnetic flux surfaces due to mechanisms arising from the electromagnetic fields. The role of the poloidal magnetic field component is to allow for an equilibrium by counteracting these drifts. One of them, the so called *gradient B drift*, is caused by the radial gradient in the magnetic field due to the compression of the field lines on the inside of the torus. The radius of gyration, also known as the Larmor radius, varies with the magnetic field strength:

$$r_g = \frac{mv_{\perp}}{|q|B}, \quad (2.1)$$

where m is the particle mass, v_{\perp} is the component of the velocity perpendicular to the direction of the magnetic field and B is the strength of the magnetic field. The Larmor radius is minimum on the high field side (the inner side of the torus) and maximum on the low field side (the outside). This causes the particle to drift in the vertical direction. Since the ions and the electrons gyrate anti-parallel to each other they also have different drift directions, creating a charge separation with an associated electric field.

Another drift mechanism, known as *curvature drift*, is a result of the curvature of the field lines and is in the same direction as the gradient B drift. As a charged particle moves along a curved magnetic field line it experiences a centrifugal force due to the field curvature that results in a drift perpendicular to both the centrifugal force and the magnetic field. Since the electrons and the ions have opposite signs of their charge, the

curvature drift will drive the particles in opposite directions.

The electric field accelerates and slows down the gyrating particles on the upward and downward part of their orbit, resulting again in longer or shorter gyration radii and an outward drift of the particle, known as $\mathbf{E} \times \mathbf{B}$ drift. This drift acts in the same direction for ions and electrons since it is independent of charge. Hence, this drift can lead to a macroscopic movement of the plasma.

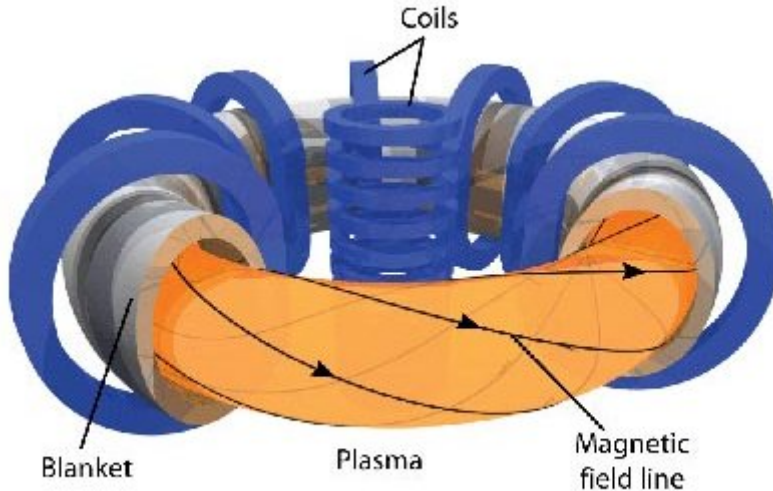


Figure 2.3: Schematic view of a typical tokamak. The plasma is confined by magnetic field lines running helically around the toroidal axis. Adapted from [6].

A stable plasma equilibrium can be obtained by twisted magnetic field lines by superimposing toroidal and poloidal field components. Magnetic field lines wrap around the torus axis in a helix and constrain the path of the charged particles, to counteract the drift effects. In a tokamak the toroidal component is generated by poloidal magnetic coils wound around the torus. The poloidal magnetic field contribution is induced by driving a current in the plasma. Figure 2.3 shows a schematic view of the tokamak concept. The field lines trace out magnetic surfaces referred to as flux surfaces of constant particle pressure which the currents flow within. Both the poloidal and the toroidal magnetic field in a tokamak scales roughly as the inverse of the major radius R and the poloidal field is significantly smaller than the toroidal magnetic field.

At the densities and temperatures reached in fusion plasmas, signif-

icant kinetic pressure is obtained in the plasma core and large pressure (p) gradients produce strong forces on the plasma. The ∇p forces are balanced by $\mathbf{j} \times \mathbf{B}$ forces arising from the magnetic field interacting with toroidal and poloidal plasma current density (\mathbf{j}). This force balance is known as the magnetic equilibrium.

2.2 Toroidal plasma current

The poloidal magnetic field can be generated by using the plasma as a secondary circuit in a transformer. In this setup the plasma acts as a single secondary loop generating the poloidal magnetic field. A large current is induced in the plasma itself, which is an excellent electric conductor. This plasma current produces heat, just as a wire warms up when an electric current flows through it. To reach *ignition*, a self sustained plasma by power release from its own fusion reactions, the fuel must be heated to around 100 million degrees. Maintaining the plasma at this temperature requires control of its density and reduction of the heat losses. As a result from any electron heating process, the resistance of the medium decreases with the temperature as $T_e^{-3/2}$, where T_e is the electron temperature. Consequently, Ohmic heating is a convenient method in the beginning of a discharge, but it becomes inefficient at higher temperatures and additional methods must be implemented.

The inductive voltage in the plasma is the time derivative of the total flux (ϕ_p) [7], i.e. the sum of the variation of stored magnetic energy and the Ohmic power. Thus, the voltage is:

$$V_{ind} = -\frac{d}{dt}(\phi_p) = V_{loop} + \frac{1}{I_p} \frac{d}{dt}(E_{magn}), \quad (2.2)$$

where $E_{magn} = \mu_0 R l_i I_p^2 / 4$ is the internal magnetic energy, μ_0 is the vacuum permeability, I_p is the plasma current, R is the major radius and l_i is the internal inductance. $V_{loop} = P_{ohm} / I_p$ is the resistive part of the voltage. In operation with constant plasma current, so called current flattop, the second term in Eq. 2.2 vanishes.

As a result of the curl of the toroidal electric field (\mathbf{E}) inductive current drive can only work temporarily. This is clear from Faraday's law $\nabla \times \mathbf{E} = -\partial \mathbf{B} / \partial t$, which states that a constant electric field can only be maintained by a time-varying magnetic field. The finite flux swing of the transformer combined with the finite resistivity of the plasma results in a pulsed tokamak operation. For steady state operation, which

is highly desirable, the poloidal component of the magnetic field must therefore be induced by non-inductive means.

2.3 Current drive methods

Current drive in a tokamak refers to the generation of a toroidal electric current flowing inside the plasma to generate a poloidal magnetic field. The required plasma current is partly self-generated and any additional current must be externally enforced. The additional current can be generated through inductive and non-inductive methods.

The self-generated part is known as the bootstrap current [8]. It arises as a consequence of collisions between particles in a curved magnetic field. Particles with a small velocity parallel to the direction of the magnetic field lines (v_{\parallel}) compared to their total energy can be trapped in the magnetic field minima, due to reflection from the mirror force from the magnetic field gradient:

$$\dot{v}_{\parallel} = -\mu \nabla_{\parallel} B, \quad (2.3)$$

where the magnetic moment $\mu = v_{\perp}^2/2B$ is an adiabatic invariant. A particle is trapped if

$$\frac{v_{\parallel,0}}{v_{\perp,0}} \leq \sqrt{B_{max}/B_0 - 1}, \quad (2.4)$$

where $v_{\parallel,0}$ and $v_{\perp,0}$ is the parallel and perpendicular velocity defined where the magnetic field is minimum on a given flux-surface (B_0) and B_{max} is the maximum magnetic field value. The trapped particles bounce back and forth on the low field side, resulting in banana shaped guiding center orbits in the poloidal projection. In the case of a finite density gradient there is an asymmetry between the co- and counter-current moving trapped electrons, resulting in a net current known as the banana current. The bootstrap current is then generated through collisions between the trapped and passing particles.

As explained in the previous section, for continuous tokamak operation additional current must be added through external means, e.g. through neutral beam injection (NBI) or resonant interaction between particles and radio-frequency (RF) waves such as the electron cyclotron (EC) wave, the ion cyclotron (IC) wave and the lower-hybrid (LH) wave. Both NBI and RF wave injection are non-inductive heating and current

drive methods that can sustain a steady-state plasma. In NBI high energy neutral particle beams are injected into the plasma to transfer their energy to the plasma ions. The particle beam is generated by accelerating ions with high voltage and convert them into neutral atoms just before the injection.

The orbits of the charged particles in a tokamak are characterised by three periodic motions and their respective frequencies: the gyro-frequency for the rotation around field lines, the bounce- or transit frequency for the parallel motion along the field lines and the drift frequency across magnetic field lines. By appropriately choosing the frequency and the launching characteristics of RF waves, it is possible to control the resonant interaction of these waves with electrons or ions. RF heating can be used to target particles of specific species and characteristics such as location, energy and magnetic moment.

Chapter 3

Lower Hybrid Current Drive

During steady-state operation in a future tokamak, the plasma current and its profile should be controlled by non-inductive methods to complement the self-generated bootstrap current. The shaping of the current profile is particularly important for the control of plasma stability. The confinement and presence of magnetohydrodynamic (MHD) instabilities are strongly dependent on the safety factor profile, a measurement of the changed toroidal angle ($\Delta\phi$) when following a field line one poloidal turn (2π):

$$q = \frac{\Delta\phi}{2\pi}. \quad (3.1)$$

For a large aspect ratio ($R \gg a$) circular tokamak the safety factor can be estimated as $q(r) \simeq rB_\phi/R_0B_\theta$ [1], where the poloidal magnetic field is proportional to the current density ($B_\theta = \mu_0 j(r)/2\pi r$). Consequently the q -profile, being inversely proportional to the current profile, can be controlled by current drive methods. Better energy confinement is obtained when the current profile is peaked away from the magnetic axis [9]. The q -profile being inversely proportional to the current profile, such scenarios correspond to a non-monotonic safety factor profile. Operation in this so called reverse magnetic shear has shown improved energy confinement and tends to facilitate steady state operation [10].

For years lower hybrid current drive (LHCD) has proven to be the most successful non-inductive current drive method with great prospects for future tokamaks [11]. One of the main advantages is its capability to drive off-axis current, which is useful for suppressing MHD instabilities

and to enable continuous operation [12]. Ever since the first demonstration of the current drive with lower hybrid waves in the Japanese JFT2 [13] and American PLT [14] the LHCD technology has been developed and used in several tokamak experiments.

Lower hybrid waves, in the frequency range between ion and electron cyclotron frequencies ($\omega_{ci} < \omega_{LH} < \omega_{ce}$), interact with electrons via Landau damping through the wave-particle resonance condition $v_{\parallel}/c = 1/n_{\parallel}$, where v_{\parallel} is the velocity of the resonant electrons and n_{\parallel} is the parallel refractive index of the wave. By injecting waves with asymmetric n_{\parallel} spectrum LH waves can be used for current drive. The frequency band of lower hybrid waves reaches between 1 and 10 GHz, corresponding to free space wavelengths in the microwave region. The group velocity of the LH wave is perpendicular to the wave vector and at the same time almost parallel to the magnetic field. The LH wave propagates with a small angle with respect to the magnetic field lines and can encircle the torus several times before reaching the plasma center. The electron cyclotron wave mainly transfers perpendicular momentum to the electrons and therefore electrons off-axis tend to become trapped, resulting in a reduced current drive efficiency. Unlike the electron cyclotron wave, the lower hybrid wave maintains a high current drive efficiency when the power is deposited far off-axis. The dispersion relation for wave propagation in the plasma can be written [15]:

$$\mathbf{D} \cdot \vec{E} = \vec{k} \times (\vec{k} \times \vec{E}) + \frac{\omega^2}{c^2} \varepsilon \cdot \vec{E} = 0, \quad (3.2)$$

where \vec{k} is the wave vector, \vec{E} is the wave electric field and the cold-plasma dielectric tensor (ε) is:

$$\varepsilon = \begin{pmatrix} \varepsilon_{\perp} & i\varepsilon_{xy} & 0 \\ -i\varepsilon_{xy} & \varepsilon_{\perp} & 0 \\ 0 & 0 & \varepsilon_{\parallel} \end{pmatrix},$$

with

$$\begin{aligned} \varepsilon_{\perp} &= 1 - \sum_s \frac{\omega_{ps}^2}{\omega^2 - \omega_{ps}^2}, \\ \varepsilon_{xy} &= \sum_s \frac{\omega_{ps}^2 \Omega_{cs}}{(\Omega_{cs}^2 - \omega^2)\omega}, \\ \varepsilon_{\parallel} &= 1 - \sum_s \frac{\omega_{ps}^2}{\omega^2}. \end{aligned}$$

Here the gyro-frequency $\Omega_{cs} = qB/m_s$ and the plasma frequency is $\omega_{ps} = (n_s q^2 / \epsilon_0 m_s)^{1/2}$. The wave equation will have a non-vanishing solution only if the determinant of \mathbf{D} is zero. From the plasma dielectric tensor one can obtain the general dispersion relation:

$$\begin{vmatrix} \epsilon_{\perp} - n_{\parallel}^2 & i\epsilon_{xy} & n_{\perp}n_{\parallel} \\ -i\epsilon_{xy} & \epsilon_{\perp} - n_{\perp}^2 - n_{\parallel}^2 & 0 \\ n_{\perp}n_{\parallel} & 0 & \epsilon_{\parallel} - n_{\perp}^2 \end{vmatrix} = 0. \quad (3.3)$$

The parallel component of the refractive index (n_{\parallel}) is set by the launcher, but varies along the propagation in the plasma. As the wave propagates in the plasma the variation in magnetic field and density will vary and Eq. 3.3 can be solved for n_{\perp} . The wave can propagate as long as $n_{\perp}^2 > 0$. Wave resonance occurs when $n_{\perp} \rightarrow \infty$ in the form of absorption. When $n_{\perp} \rightarrow 0$ the wave is reflected. The two solutions of the above relation are known as the fast and the slow wave, having a component of the electric field perpendicular and parallel respectively to the magnetic field.

Waves with $|n_{\parallel}| > 1$ can couple to the plasma if the density is above the cut-off density. At the plasma edge the LH wave is evanescent and placement of the LH launcher close to the plasma edge is required for efficient coupling. Coupling of the power to the plasma requires that the density in front of the antenna is above the cut-off density or that the evanescent region between the antenna and the cut-off layer is small compared with the wavelength. The cut-off density is given by:

$$n_e = \frac{\omega^2 \epsilon_0 m_e}{q_e^2}, \quad (3.4)$$

where ϵ_0 is the vacuum permittivity, m_e and q_e are the electron mass and charge. For lower hybrid waves with the frequency $f = 3.7$ GHz the cut-off density is around $1.7 \times 10^{17} \text{ m}^{-3}$.

For a given density, the wave can access the plasma if the parallel refractive index of the wave ($n_{\parallel} = ck_{\parallel}/\omega$), where k_{\parallel} is the parallel component of the wave vector and c is the speed of light satisfies the accessibility condition [16]:

$$|n_{\parallel}| = \frac{\omega_{pe}}{\omega_{ce}} + \sqrt{1 + \frac{\omega_{pe}^2}{\omega_{ce}^2} - \frac{\omega_{pi}^2}{\omega^2}}. \quad (3.5)$$

For a given n_{\parallel} , Eq. 3.5 sets an upper limit for the density, above which the wave cannot propagate beyond the pedestal region.

An electron that interacts with a wave absorbs some parallel momentum ($m\Delta v_{\parallel}$) which leads to an increase of current $\Delta J = q\Delta v_{\parallel}$ and kinetic energy $\Delta\epsilon = mv_{\parallel}\Delta v_{\parallel}$. Since the goal is to drive current, rather than to heat the plasma, the ratio between energy gain and current increase $\Delta\epsilon/\Delta J$ should be minimised. This ratio is proportional to v_{\parallel} and therefore it seems more favourable to accelerate slower electrons. However, it is more efficient to accelerate the faster ones since the Coulomb collisions are less frequent at higher velocity. The characteristic collision time (τ) between electrons corresponds to the required time for cumulative small angle collisions to deflect the path of the electron by a significant angle (on the order of $\pi/2$) is:

$$\tau = \frac{4\pi\epsilon_0 m_e^2 v^3}{q_e^4 n_e \ln \Lambda}, \quad (3.6)$$

where v is the velocity of the electron relative to the thermal background and $\ln \Lambda$ is the Coulomb logarithm which is the factor by which small-angle collisions are more effective than large-angle collisions. We see that the collision time depends on both density and the velocity of the electrons. As a consequence LHCD is most efficient at low density (n_e) and high temperature plasmas. Suprathermal electrons have higher velocity relative to most other particles in the plasma (v_{th}) and are therefore less collisional. The efficiency of the current drive is therefore favoured by a low parallel refractive index (n_{\parallel}), that is high phase velocity of the wave. As the wave enters hotter regions of the plasma, the number of resonant electrons increases. Even though there are usually few electrons resonant with the wave of high phase velocity, the absorption is efficient due to the generation of a tail of energetic electrons at lower velocity than the phase velocity of the launched wave. This phenomenon is known as the spectral gap problem and can to some extent be explained by an upshift of the parallel refractive index due to refraction in the toroidal geometry as the wave travels through the plasma [18]. Additional explanations, such as spectral broadening due to density fluctuations [19] and parametric instabilities in the scrape off layer in front of the LH launcher [20], have been proposed.

The current drive efficiency is proportional to the inverse of the plasma electron density (n_e) and the inverse square of the parallel refractive index [17]. The efficiency of the current drive is defined as the ratio of the driven current (j) over the used power density (p) [21]. Since the total driven current scales as $I_{CD} \sim \pi a^2 j$, where a is the minor radius

and the total power scales as $P \sim 2\pi R\pi a^2 p$, it is convenient to define the LH current drive efficiency as

$$\eta_{20} = \frac{n_{20} \cdot R \cdot I_{LH}}{P_{LH}}, \quad (3.7)$$

where n_{20} is the central electron density expressed in units of 10^{20} m^{-3} , R is the tokamak major radius, I_{LH} is the LH driven current and P_{LH} is the input LH power (in SI units) [22]. The factor n_{20} accounts for the inverse density dependence of the non-inductively driven current. In this way the current drive efficiency η_{20} can be compared between different experiments and used for extrapolation for future tokamaks.

3.1 Landau damping

Landau damping is the absorption that occurs due to energy exchange between electromagnetic waves and particles in the plasma with velocities close to the phase velocity ($v_{ph,\parallel} = \omega/k_{\parallel}$) of the wave. The particles interact strongly with the wave and will be accelerated if they are moving slightly slower than $v_{ph,\parallel}$. In the same way particles that move faster than $v_{ph,\parallel}$ will lose energy to the wave and slow down. The absorption is known as Landau damping and the resonance condition is:

$$v_{\parallel} - v_{ph,\parallel} = 0. \quad (3.8)$$

If there are more particles with velocity below $v_{ph,\parallel}$ than there are faster particles, the number of particles that gain energy will be greater than the number of particles that lose energy, see Fig. 3.1. In other words, the wave is damped and the plasma is heated. In addition, an asymmetry in velocity distribution results from the resonance condition (Eq. 3.8), which generates a net electric current.

Due to the high efficiency of Landau damping at high temperatures ($T_e \sim 10 \text{ keV}$), in ITER the LH wave will not be able to access the center, but is absorbed in the outer parts of the plasma. The main purpose for LHCD for ITER would be as a tool for off-axis current profile control and to save volt seconds in the ramp up phase of the plasma current [24, 25].

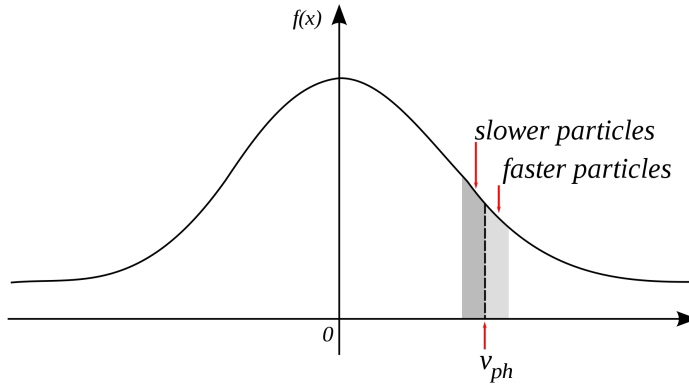


Figure 3.1: Due to the anisotropy in the velocity distribution there are fewer particles with velocity higher than the phase velocity of the wave $v_{ph,\parallel}$ which results in a net electric current. Adapted from [23].

3.2 Kinetic description

The basic difference between a gas and a plasma is that a plasma is composed of charged particles, which react to electromagnetic forces. The most complete description of a plasma composed of N particles would rely on the solution of the $3N$ equations of motion where the calculation of the force acting on each particle has to account for the influence of all the other particles in the system. Such calculations are not reasonable and moreover would generate a lot of unnecessary information about the microscopic behaviour of every particle in the system. Since we are interested in macroscopic quantities like density, temperature and currents, a statistical approach is taken. The electromagnetic fields that determine the forces on each particle are functions of the charge and current distributions in the plasma and hence of the distribution function itself. Therefore the solution of the kinetic equation is very complicated even in the collisionless limit.

The evolution of the electron distribution in a plasma is governed by the Fokker-Planck equation, a convection-diffusion equation in phase space. It describes the multiple scattering processes of the particles in the plasma. The dominant interactions are Coulomb collisions, which occur when two particles pass each other close enough to be within the so called Debye sphere, where the particle is electrostatically influenced by other charged particles. Besides collisions, the formulation can describe

wave-plasma interaction and the force on particles in an electric field. In plasma physics the Fokker-Planck equation is fundamental in heating, current drive, resonant wave-particle interaction and runaway electron dynamics.

The lower hybrid wave absorption and the distribution function are described self-consistently by solving a non-linear system where the RF waves are solutions to Maxwell's equations:

$$\nabla \times \mathbf{E} = -\frac{\partial \mathbf{B}}{\partial t}, \quad (3.9)$$

$$\nabla \times \mathbf{B} = \mu_0 \mathbf{J} + \frac{1}{c^2} \frac{\partial \mathbf{E}}{\partial t}. \quad (3.10)$$

The effect of the LH waves on the plasma depends on the electron distribution. The current is given by

$$\mathbf{J}(\mathbf{x}, t) = q \iiint \mathbf{v} f(\mathbf{x}, \mathbf{p}, t) d^3 \mathbf{p}, \quad (3.11)$$

where $f(\mathbf{x}, \mathbf{p}, t)$ is the distribution function of particles with charge q , with \mathbf{x} being the position in configuration space and \mathbf{p} is the relativistic momentum. The number of particles in the volume around the point $\mathbf{z} = (\mathbf{x}, \mathbf{p})$ at the time t is given by:

$$\int f(\mathbf{x}, \mathbf{p}, t) d^3 \mathbf{p} d^3 \mathbf{x} = N(t). \quad (3.12)$$

The movement of the particle in the plasma can be expressed as $\dot{\mathbf{z}} = (\dot{\mathbf{x}}, \dot{\mathbf{p}})$. The distribution function must satisfy the continuity equation, expressing conservation of total number of particles:

$$\frac{\partial f}{\partial t} + \frac{\partial}{\partial \mathbf{z}} (\dot{\mathbf{z}} f) = 0, \quad (3.13)$$

which when the equations of motion are divergence free is known as the Vlasov equation:

$$\frac{\partial f}{\partial t} + \mathbf{v} \cdot \nabla f + \dot{\mathbf{p}} \cdot \frac{\partial f}{\partial \mathbf{p}} = 0. \quad (3.14)$$

The electric and magnetic fields in $\dot{\mathbf{p}} = q(\mathbf{E} + \mathbf{v} \times \mathbf{B})$ include the small-scale fluctuations responsible for interaction of individual particles. In this context small-scale means less than the radius of the Debye sphere, known as the Debye length. The effects of these collisions can be included in a separate collision operator $C(f, f_\alpha)$, where α denotes all plasma

particle species, including the electrons themselves. The Fokker-Planck equation, which now includes only the macroscopic average electric (\mathbf{E}) and magnetic fields (\mathbf{B}), is the Vlasov equation with the effects of small scale fluctuations gathered in a collision term on the right hand side:

$$\frac{df}{dt} = \frac{\partial f}{\partial t} + \mathbf{v} \cdot \nabla f + \dot{\mathbf{p}} \cdot \frac{\partial f}{\partial \mathbf{p}} = C(f, f_\alpha). \quad (3.15)$$

Here $\dot{\mathbf{p}} = q(\mathbf{E} + \mathbf{v} \times \mathbf{B})$ is the Lorentz force acting on the electrons from both constant equilibrium and oscillating radio frequency electromagnetic fields. The distribution function f must be solved self-consistently with the RF waves in Eqs. 3.9 and 3.10.

In general Eqs. 3.14 and 3.15 are not easy to solve, essentially because the forces acting on the system can depend in complicated ways on the distribution function itself. Charged particles in motion constitute a current and therefore affect the electromagnetic fields. These equations are in general nonlinear integro-differential equations.

3.3 Spectral properties of launched wave

The purpose of the LH launcher is to couple the wave with the plasma as efficiently as possible. It usually consists of an array of waveguides placed side by side with a phase shift between consecutive waveguides. The characteristics of the LH power spectrum is determined by the waveguide array configuration, dimensions and phasing. The active waveguides may be alternated by passive waveguides that are short circuited but radiates power to the plasma through cross coupling at the plasma edge with the RF power emitted from the active waveguides. However, as a simple demonstration of an ideal power density spectrum calculation we consider a phased array of active waveguides, see Fig. 3.2. By dividing a waveguide into a number of secondary waveguides one obtains a multi junction grill that splits the incident power along the toroidal direction.

Each of the waveguides emit electric field with a certain power amplitude and phasing. Assuming that the electric field amplitude is constant along the toroidal direction (z) and the phasing is linear, the electric field can be expressed as:

$$E(z) = \sum_{n=1}^N E_n \Pi_n(z) = \sum_{n=1}^N A_n e^{i\phi_n} \Pi(z), \quad (3.16)$$

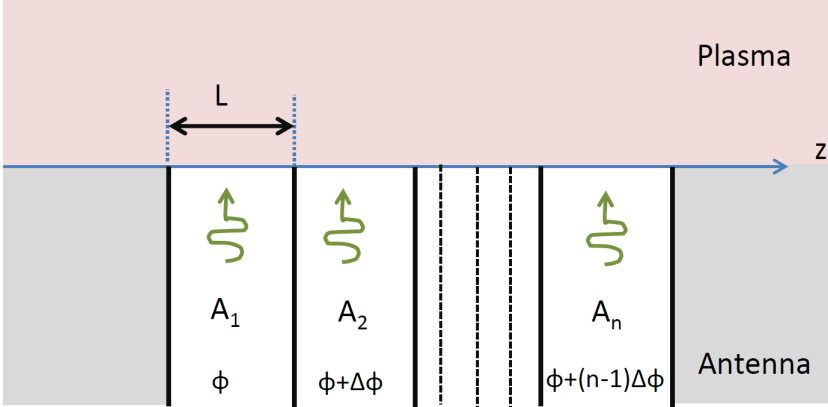


Figure 3.2: A linearly phased array of waveguides.

where A_n is the amplitude at the n^{th} wave guide and Π_n the Heaviside step function, zero everywhere but for z at waveguide openings where it is equal to unity. We assume that the waveguides radiate with linear phasing ($\phi_n = n\Delta\phi$).

Fourier transform of the power at the interface between the waveguides and the plasma edge gives the power spectrum as a function of the refractive index in the toroidal direction ($n_z = k_z/k_0$). The power spectrum is given by:

$$\tilde{E}(k_z) = \int E(z)e^{ik_z z} dz = \text{sinc}(n_z k_0 L/2) \sum_{n=1}^N (e^{in\phi_n} e^{ink_0 n_z L}), \quad (3.17)$$

where $k_z = n_z k_0$. The modulus square of $\tilde{E}(k_z)$ is proportional to the power spectrum:

$$\frac{dP}{dn_z} = \text{sinc}^2(n_z k_0 L/2) \left(\frac{\sin(N\phi/2)}{\sin\phi/2} \right)^2, \quad (3.18)$$

with $\phi = k_0 n_z \Delta z - \Delta\phi$. The above expression is maximised at $\phi = 2p\pi$ which gives the main refractive index (for $p = 0$):

$$n_{z0} = \frac{\Delta\phi}{k_0 \Delta z} = \frac{\Delta\phi}{k_0 L}. \quad (3.19)$$

If in addition one accounts for the number of modules in the multi-junction and assumes $n_z \approx n_{\parallel}$, i.e. the magnetic field lines are assumed

to be parallel to the toroidal direction, the main parallel refractive index may be tuned around the nominal value. The launcher will operate with a phase shift $\delta\Phi$ between two modules, resulting in a main parallel refractive index:

$$n_{\parallel 0} = \frac{\Delta\phi}{k_0 L} + \frac{\delta\Phi}{N k_0 L}, \quad (3.20)$$

where N is the number of active waveguides per module.

Contrary to the phase shift $\Delta\phi$ between two active waveguides of a module, which is fixed by the waveguide geometry, the phasing between two adjacent modules $\delta\Phi$ can be changed, by modifying the phase at the klystron, which tunes the parallel refractive index at the power peak value. Thus $n_{\parallel 0}$ is fixed around the design value, set by geometry, with some degree of flexibility by modifying the nominal phase shift between two modules.

The directivity of the launcher compares the radiation intensity in a particular direction, parallel and antiparallel to the magnetic field, with the total coupled power (P). In the case of LHCD studies, it is useful to define the directivity as the ratio of the part of the spectra with co-current driving n_{\parallel} over the total power. Waves with $|n_{\parallel}| < 1$ cannot couple to the plasma and therefore the limit of integration starts from $|n_{\parallel}| = 1$. The directivity can be defined as:

$$D = \frac{1}{P} \int_1^{\infty} P(n_{\parallel}) dn_{\parallel}. \quad (3.21)$$

Since the driven current is proportional to the inverse square of n_{\parallel} , in addition to the above definition of directivity, it is also useful to quantify the quality of the spectra, by defining a n_{\parallel}^2 weighted directivity for current drive (D_{cd}) according to the following equation:

$$D_{cd} = (1 - RC) \times \frac{n_{\parallel 0}^2}{P} \left(\int_1^{\infty} \frac{1}{n_{\parallel}^2} P(n_{\parallel}) dn_{\parallel} - \int_{-\infty}^{-1} \frac{1}{n_{\parallel}^2} P(n_{\parallel}) dn_{\parallel} \right), \quad (3.22)$$

where RC is the average reflection coefficient in front of the launcher modules and $n_{\parallel 0}$ is the refractive index of the main lobe.

Chapter 4

Modelling of LHCD for Tore Supra plasmas

For the purpose of long pulse discharges, Tore Supra is equipped with two LH launchers designed to drive current during 1000 s long pulses. Ever since the start up, LHCD has been an important part of the research at Tore Supra. Its well developed system for non-inductive current drive is described in Sec 4.1. Among tokamaks, Tore Supra holds the record of injected energy, with LH power alone, with a total of 1 GJ from a six minute long discharge [26]. More recently, a 950 MJ discharge was performed, at higher LHCD power than before (5.3 MW) thanks to the upgraded LHCD power capability [12]. The overall world record of injected energy is held by the Large Helical Device (LHD) stellarator (1.6 GJ) [27].

Due to limitations in measurement of the current profile and other moments of the distribution function, numerical modelling is essential in order to understand and analyse the effect of LHCD on the electron distribution function. Such tools enable detailed analysis of current drive properties in experiments as well as predictive modelling for future machines. In this thesis the effect on the distribution function of LH waves coupled to the plasma with the two launchers Fully Active Multijunction (FAM) and Passive Active Multijunction (PAM) is modelled. For this purpose a set of well established codes developed for tokamak studies at CEA are specifically coupled and optimised for modelling the process of LHCD, including a code for equilibrium and transport (METIS) [28], LH wave coupling to the plasma (ALOHA) [29], LH wave propagation through ray-tracing (C3PO) [30] and the power absorption on

the electron distribution through a Fokker-Planck solver (LUKE) [31]. The modelling scheme is presented in Fig. 4.1. In Sec. 4.2 the codes in the LHCD modelling suite are briefly introduced. More detailed descriptions of the codes are found in the above references. Finally the LHCD modelling is validated by fast electron bremsstrahlung emission (FEB) reconstruction with the R5X2 code [32]. For a more complete description of the diagnostics, see Ref. [33].

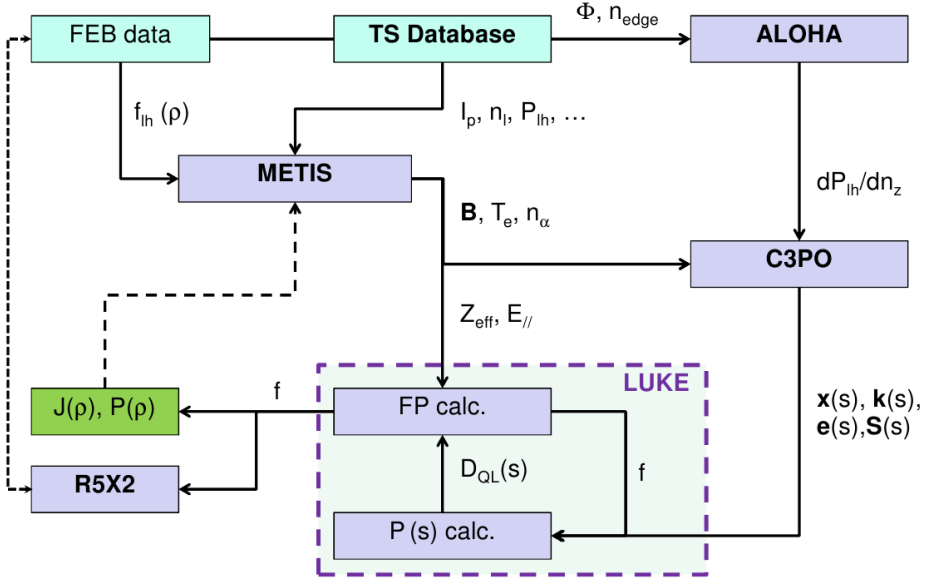


Figure 4.1: Modelling scheme for LHCD in Tore Supra.

4.1 The LHCD system in Tore Supra

LHCD has been used in Tore Supra for current drive for more than 20 years. Over the years, different launcher concepts have been tested. A new LHCD launcher that relies on a periodic combination of active and passive waveguides was installed in Tore Supra in 2009 [34], [35]. Designed with ITER-relevant scenarios in mind, the PAM launcher allows efficient active cooling of the waveguides, necessary for long pulse operation [36], [34]. The PAM launcher has shown encouraging experimental results, with reflection coefficient and power handling that meet the expectations for an ITER-relevant LH launcher [22].

As a complement to the PAM launcher an older launcher (FAM) of

different design is installed in Tore Supra. The FAM launcher consists of only active waveguides in each module with a passive waveguide inserted between the modules, see Fig. 4.2. Figure 4.3 shows the launchers from the inside of the tokamak.

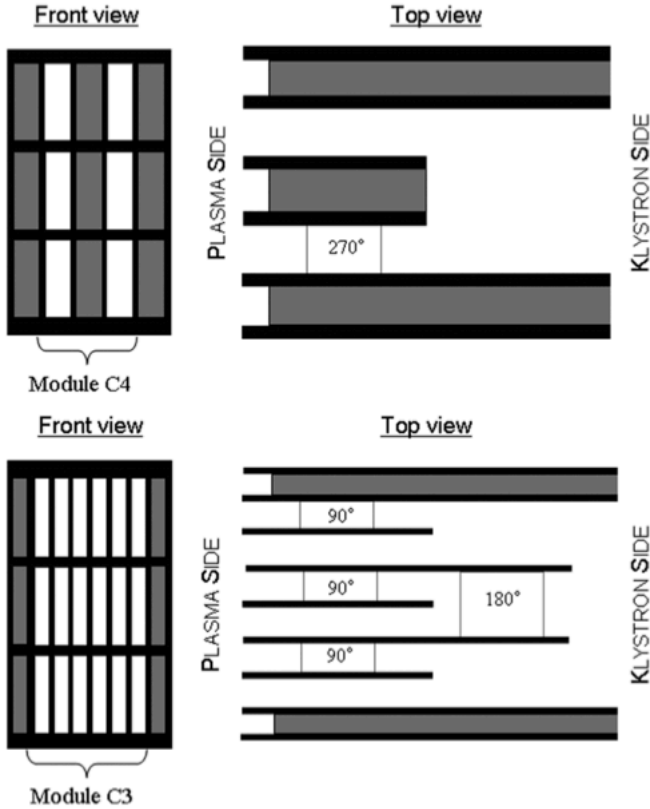


Figure 4.2: Schematic front and top view of PAM, also denoted C4 (top) and FAM, also denoted C3 (bottom). The grey rectangles correspond to passive waveguides and the white rectangles to active waveguides. Each module consists of three rows of waveguides. Adapted from [37].

The power of the LH system is generated by 16 klystrons, eight for each launcher, operating at 3.7 GHz. Transmitted through about 20 meter of rectangular copper waveguides to the edge of the tokamak, the power is split in two in each waveguide in a 3 dB hybrid junction. This results in 16 transmission lines for each launcher, out of which eight lead to the upper and eight to the lower part of each launcher.



Figure 4.3: PAM (left) and FAM (right) launchers seen from the inside of Tore Supra.

Mode converters (TE10 to TE30) divide the incoming power into three poloidal rows for each of the two half launchers. The waveguide modules are connected to the tokamak through double BeO windows. Figure 4.4 gives an overview of the setup.

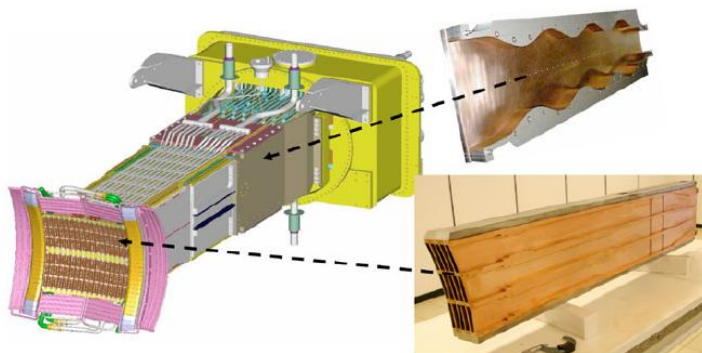


Figure 4.4: Complete PAM type launcher setup including the mode converter and a PAM module.

The PAM launcher consists of 16 modules with eight active and eight passive waveguides each. The multijunction design results in a low fraction of reflected power ($< 2\%$) from the plasma for densities near the cut off ($1.7 \cdot 10^{17} \text{ m}^{-3}$ at $f = 3.7 \text{ GHz}$) in front of the launcher mouth [36].

This makes PAM type launchers very advantageous for ITER, where the density at the launcher mouth is low due to significant distance between the plasma edge and the wall.

The LH wave launchers are designed for long pulse operation in order to enable research on steady-state plasma control. The multijunction launchers, also known as grills, consist of phased arrays of waveguides that produce waves propagating with phase velocity $v_{\parallel} = c/n_{\parallel}$ parallel to the magnetic field. The wave is launched with a spectrum of velocities, for convenience expressed in n_{\parallel} . As described in Sec. 3.3, the main features of the power spectrum are fixed by geometry, but the peaks of the spectrum can be slightly tuned by modifying the phase shift between the modules. The main peak, $n_{\parallel 0}$, of the launched power spectrum for PAM can be adjusted according to the expression:

$$n_{\parallel 0} = \frac{\Delta\phi}{k_0 L} + \frac{\delta\Phi - 180^\circ}{N_{wg} k_0 L \times \frac{180}{\pi}} = 1.72 + \frac{\delta\Phi - 180^\circ}{N_{wg} k_0 L \times \frac{180}{\pi}}, \quad (4.1)$$

where the number of active waveguides per module is $N_{wg}^{C4} = 2$, $k_0 = 77.54 \text{ m}^{-1}$ at the operation frequency 3.7 GHz, the geometric periodicity of the waveguide array is $L^{C4} = 35.25 \text{ mm}$ and the phasing between two active waveguides in a module in C4 is $\delta\phi = 270^\circ$.

The nominal phase shift is $\delta\Phi = 180^\circ$ for the C4 launcher. At this phasing the directivity, i.e. the ratio of the co-driving and the total coupled power, is maximised around the cut-off density [37]. The C4 launcher is most efficient for a main peak centered around $n_{\parallel} = 1.7$. C3 is optimal for current drive with phasing such that the main peak is centred at $n_{\parallel} = 2.0$.

4.2 LHCD modelling

In this section, the codes of the LHCD modelling chain are briefly described in the order of their appearance in the workflow presented in Fig. 4.1.

4.2.1 Core plasma modelling (METIS)

The global discharge evolution and equilibrium profiles for each plasma scenario are obtained from the fast integrated tokamak simulator METIS (Minute Embedded Tokamak Integrated Simulator). METIS provides

interpretative simulations of Tore Supra discharges yielding particle and impurity densities, ion and electron temperature profiles, bootstrap current and plasma momentum. It also provides the electric field parallel to the magnetic field lines radial profiles ($E_{\parallel}(r)$), used for simulation of inductive pulses [28].

The METIS code computes the time evolution of the global plasma quantities for given waveforms of the control parameters. It solves the current diffusion equation assuming an approximate equilibrium evolution. The temperature and density profiles are fitted from experimental data from the Tore Supra database. In LH scenarios, METIS requires an initial guess of the radial current profile, more precisely of the form factor $f_{LH}(\rho)$ in the current profile decomposition $J_{LH} = \eta_{LH} f_{LH} P_{LH}$ where η_{LH} is the current drive efficiency and P_{LH} the lower hybrid power. The current drive efficiency η_{LH} is adjusted by matching the edge poloidal flux evolution with experimental measurements. The initial guess of the radial profile has routinely been based on the Abel inverted FEB emission profile in the energy range 60 – 80 keV. Alternatively it can be prescribed by the user. The shape of the FEB profiles provides an acceptable initial guess for FAM driven scenarios since the power deposition profiles coincide with the current profiles, while it is generally not the case for PAM driven scenarios because of characteristics in the LH spectrum. This was one of the main results of [paper A](#) and is discussed therein. The quality of a simulation is assessed by comparing the METIS calculated internal inductance (l_i) with experimental measurements. The best result is obtained when the LUKE calculated form factor of the current profile is iteratively put in to the METIS calculations, a result which is discussed in [paper A](#).

4.2.2 LH wave coupling (ALOHA)

Detailed spectra based on experimental measurements of phase and LH power from the Tore Supra database are produced for each scenario and launcher with the Advanced Lower Hybrid Antenna (ALOHA) code. ALOHA models the coupling of LH slow (transverse) and fast (longitudinal) waves between the radiating waveguide structures and the plasma edge. The output is a power spectrum of parallel refractive index. In our simulations we use the ALOHA-1D version which calculates the coupling between one toroidal waveguide row of the launcher for the slow wave, as opposed to the ALOHA-2D version which calculates the coupling between all the waveguide rows for the slow and the fast wave. The 1D

version is faster (minutes as opposed to hours) and agrees well with the 2D version in the type of scenarios in question [29].

The reflection coefficient is computed by treating the plasma as an antenna load. The antenna used in simulations is defined by waveguide dimensions and module excitation. The plasma edge is defined as input, by specifying the electron edge density profile defined by two density gradient scale lengths, see Fig. 4.5. For a given scenario, the density at the edge can be estimated from Langmuir probe measurements or by matching the ALOHA obtained reflection coefficient with experimental measurements. Eight Langmuir probes, placed in the corners of each

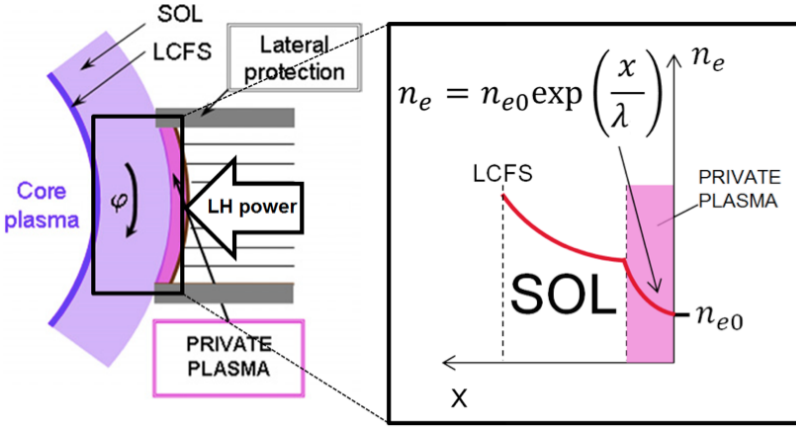


Figure 4.5: Toroidal view of the first private plasma region, limited by the two lateral protections. The electron density profile in front of the LH launcher is described with two plasma layers. The Langmuir probes yield the density in the region between the waveguide mouths and the tip of the side protection, i.e. in the private plasma.

of the two launchers, measure the local plasma density in front of the launchers. To protect the launcher from high heat and particle flux there are two lateral protection components (limiters) placed a distance $d = 2$ mm from the launcher face. The layer of a low density plasma between the launcher face and the limiters is called the private plasma. The Langmuir probes measure in the private plasma that is formed between the LH launcher mouth and the scrape off layer (SOL), see Fig. 4.5. In the private plasma layer the density varies approximately as

$$n(x) = n_{Langmuir} e^{\frac{(x-d)}{\lambda}}, \quad (4.2)$$

where x is the position relative to the launcher mouth, $d = 2$ mm the distance between the SOL and the launcher mouth and λ is the density gradient scale length ($\lambda = 2$ mm is used in the ALOHA calculations), see Fig. 4.5. The density at the launcher mouth can thus be assumed to be between $n_{Langmuir}/e$ and $n_{Langmuir}$. Current drive calculations are expected to be sensitive to such a density error, since the n_{\parallel} weighted directivity and reflection coefficient vary significantly in the relevant density region, see Fig. 4.6. The edge density is therefore an important initial condition in the LHCD modelling that affects the distribution of power between most powerful positive and negative lobes rather than the position of these lobes. This is demonstrated in Fig. 4.7 where the spectra for two different values of the edge density are compared.

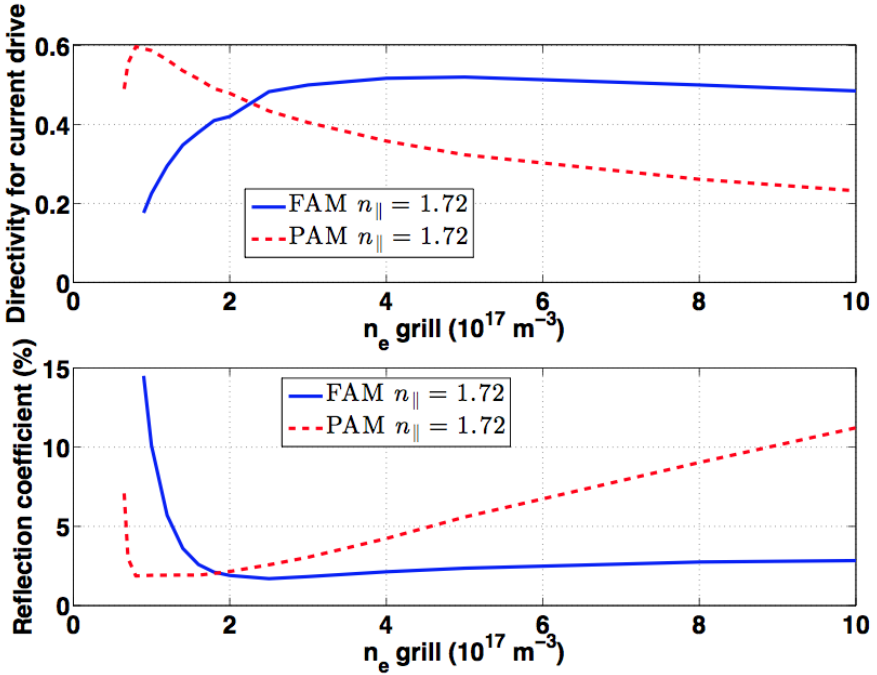
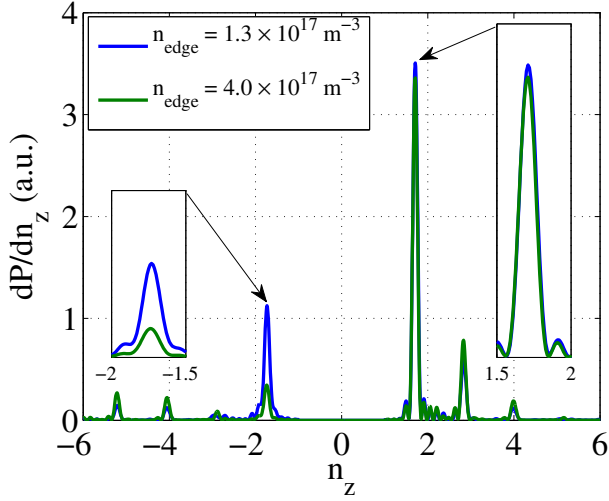
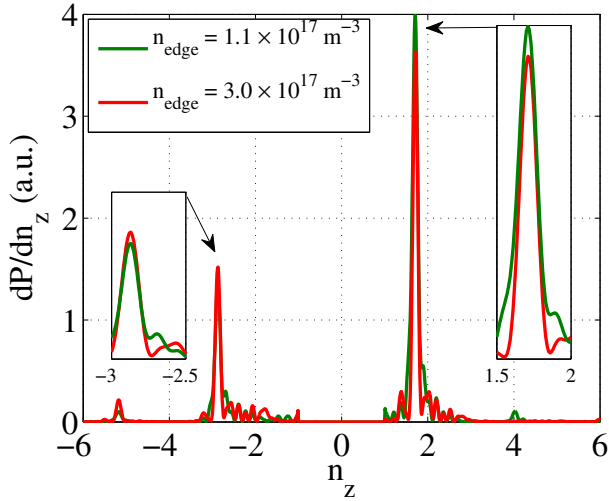


Figure 4.6: The directivity for current drive and reflection coefficient for FAM (blue) and PAM (red) launcher with module phasing corresponding to a main parallel refractive index at 1.72, calculated in ALOHA.

To some degree the fine details of the spectra used for the LHCD calculations can be simplified, to reduce computational effort while keeping details significant for the current drive. The number of rays in a wave



(a)



(b)

Figure 4.7: The launched LH spectrum calculated by ALOHA with two different values of the edge density at the antenna mouth for (a) FAM launcher, and (b) PAM launcher. The edge density used in ALOHA calculations of the spectra is defined either by Langmuir probe measurement (the higher density value) or by matching the RC from measurements with ALOHA with the corresponding density (the lower density value).

used in the simulations is given by the product of number of lobes in the launched spectrum and the number of vertical positions or waveguide rows. Systematic scans of the number of poloidal launching positions and number of rays values used in the ray-tracing calculations are done. It is found that 36 rays, corresponding to the six waveguide rows and the six main lobes in the LH spectrum, fitted to Gaussian lobes, are sufficient to describe the LH wave propagation from the FAM and PAM launchers.

4.2.3 Ray-tracing/Fokker-Planck (C3PO/LUKE)

The C3PO/LUKE module is designed to describe the propagation and absorption of RF electron resonant waves, such as lower hybrid and electron cyclotron waves. Both the ray-tracing code C3PO and the 3D bounce averaged relativistic Fokker-Planck solver LUKE consider arbitrary axisymmetric magnetic equilibrium in a curvilinear coordinate system (ψ, θ, ϕ) , where ψ is the poloidal flux coordinate and θ and ϕ are the poloidal and toroidal angles respectively. The wave propagation is modelled with the C3PO code by a series of rays with initial parameters through ray-tracing technique. The propagation and linear absorption of the launched LH waves in the tokamak are calculated using a cold-plasma dielectric tensor. The ray-tracing description is based on the validity of the WKB approximation with the condition $\lambda \ll L$, where λ is the LH wavelength and L is the length scale of the equilibrium variation [38]. Also, the rays must satisfy $\Delta n_{\parallel} \ll |n_{\parallel}|$, i.e. the rays must be well collimated. If these conditions are not fulfilled, a full wave approach must be taken [39].

The ray propagation is followed until all the RF power is linearly absorbed. Once the ray trajectories are solved linearly the LUKE code calculates the quasi-linear absorption of the LH power by self-consistently solving the power transport equation along each ray on the 2D fast electron distribution function in momentum space [31]. LUKE applies a relativistic, momentum conserving, linearised collision operator. A quasi-linear collision operator (D_{QL}) is applied to calculate the LH wave absorption. The LUKE code solves the evolution of electron distribution, and its moments such as power deposition and current profile. The effect of magnetically trapped particles is also accounted for [40]. Full convergence is obtained in the self-consistent calculation of the wave damping and distribution function. In Tore Supra the damping rate of the LH wave is low and consequently quasilinear effects on the damping

are significant. For ITER, due to the high temperature, the spectral up-shift is stronger and the scenarios are in a linear wave damping regime [40].

The wave equation for the RF fields $\tilde{\mathbf{E}}(\mathbf{x}, t)$ and $\tilde{\mathbf{B}}(\mathbf{x}, t)$, solved explicitly by C3PO is [31]:

$$\nabla_{\mathbf{x}} \times \nabla_{\mathbf{x}} \times \tilde{\mathbf{E}} + \mu_0 \sigma(f) + \frac{\partial \tilde{\mathbf{E}}}{\partial t} + \frac{1}{c^2} \frac{\partial^2 \tilde{\mathbf{E}}}{\partial t^2} = 0, \quad (4.3)$$

where σ is the conductivity tensor that linearly operates on f . The evolution of the distribution function $f(\mathbf{x}, \mathbf{v}, t)$ is solved by the bounce-averaged guiding center Fokker-Planck equation:

$$\frac{df}{dt} = \frac{\partial f}{\partial t}|_C + \frac{\partial f}{\partial t}|_E + \frac{\partial f}{\partial t}|_{RF} + \frac{\partial f}{\partial t}|_T, \quad (4.4)$$

where the terms on the right hand side of Eq. 4.4 represent:

- $\frac{\partial f}{\partial t}|_C$ is the collision operator of the collisions between electrons and the different plasma species, including the electrons themselves.
- $\frac{\partial f}{\partial t}|_E$ is the inductive parallel electric field driven acceleration.
- $\frac{\partial f}{\partial t}|_{RF}$ is the term of RF wave-particle interaction.
- $\frac{\partial f}{\partial t}|_T$ is a term for radial transport (proportional to the diffusion coefficient D_r).

4.2.4 FEB reconstruction (R5X2)

The effects of LH waves modelled by METIS/ALOHA/C3PO/LUKE on the electron distribution function are validated against experimental data from the Tore Supra tokamak. The best diagnostic for the fast electron physics is provided by FEB emission measured by the hard X-ray (HXR) cameras. HXR spectroscopy provides information about the power deposition profile in the plasma but a reconstruction of the electron distribution from the emission is not possible due to the complete mixing between angular, radial and momentum dependence of the fast electron tail [31]. A synthetic diagnostic of the bremsstrahlung emission from suprathreshold electrons by the code R5X2 allows for a comparison of the LHCD simulation with experimental measurements. The HXR deconvolution is an ill conditioned problem, which makes R5X2 an important synthetic tool, yielding a line integrated emission based on the

specifications of the HXR tomographic detection system [41]. The FEB reconstruction allows for direct comparison of count rate and photon temperature.

The code R5X2 reconstructs the local emissivity of non-thermal bremsstrahlung from LH generated fast electrons in an arbitrary axisymmetric magnetic configuration using Legendre polynomial decomposition [32]. Bremsstrahlung emission in the HXR photon energy lies in the energy range 30–200 keV, but due to Compton scattering effects and count rate statistics it is only relevant to detect photons in the energy range 50 – 110 keV. In R5X2 the bremsstrahlung emission is reconstructed as a function of chord number, yielding an output which is directly comparable to the experimental HXR data. Comparison between simulations and HXR profile is used for validation of the modelling and in addition quantifies the order of fast electron radial transport, a debated topic in fusion research.

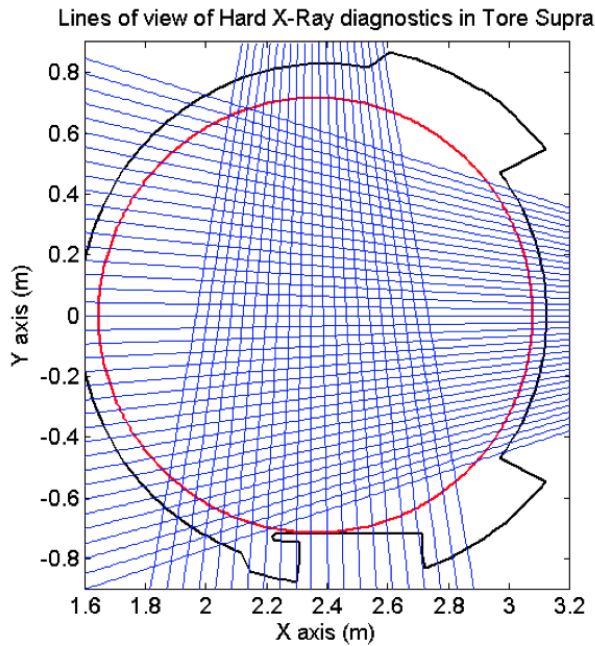


Figure 4.8: Schematic view of the hard X-ray tomographic system in Tore Supra. The lines of sight of the detectors, also called chords, are marked in blue.

The diagnostics consist of one vertical and one horizontal camera equipped with neutron shielding and respectively 21 and 38 cadmium

telluride (CdTe) detectors, see Fig. 4.8. Each detector measures the HXR in a poloidal section of the plasma, integrated along the line of observation. Given the detector response function, a count rate signal is retrieved for each chord. Abel inverted FEB emission profiles in the energy range $60 < E < 80$ keV have routinely been used as a relative measurement of the radial current profile for the lower hybrid driven current in Tore Supra. The amplitude is rescaled according to a current drive model. As thoroughly discussed in [paper A](#), the interpretation of the Abel inverted FEB emission profiles as a measurement of the current profile, is valid for the FAM type launcher but not for the PAM launcher.

4.2.5 Summary of LHCD modelling

Several pulses have been modelled with the LHCD simulation suite, for current driven by the FAM and/or PAM launcher currently installed in Tore Supra. Two typical full current drive scenarios driven with FAM (#31527) and PAM (#45525) presented in [paper A](#) provide an illustration of the modelling workflow and lead to interesting conclusions on the current drive properties of the two LH launchers. In particular, it was found that details in the launched asymmetric LH spectra are different for the two launchers. Launched waves from the two launchers with main lobes positioned at the same n_{\parallel} value result in different current profiles, due to differences in the secondary lobes launched in opposite directions with respect to the main lobes. For the FAM launcher, the most powerful secondary lobe in the opposite direction is located at the same value of $|n_{\parallel}|$ as the main lobe (see Fig. 4.7(a)). The associated power is therefore deposited at the same radial location as the main lobe. As a consequence, the current profile and the power deposition profile generally coincide for the FAM launcher. In the PAM spectrum, the most powerful secondary lobe in the opposite direction is found at a different value of $|n_{\parallel}|$ than the main lobe (see Fig. 4.7(b)) and is absorbed more off axis than the power from the main lobe. Therefore the current profile does generally not have the same shape as the power deposition profile. Because the perpendicular FEB emission does not depend on the toroidal direction of the emitting electron, the radial FEB profile is more representative of the power deposition profile than the current profile. The Abel inverted FEB profiles in the energy interval 60 – 80 keV have routinely been used as estimates of the LH current profile for FAM driven scenarios. This estimation is however not valid in PAM scenarios, since the current and power absorption profiles generally differ significantly.

Previous current drive simulations of Tore Supra discharges with Fokker-Planck codes have systematically overestimated the current drive efficiency for FAM driven scenarios. Given experimental evidence that the LH power is indeed properly coupled to the plasma, and since the directivity of FAM spectra is very sensitive to the edge density when close to the LH wave cut-off, a possible explanation is that the edge density has been systematically overestimated (see Fig. 4.6). In the present work, the edge density was obtained by matching the reflection coefficients from ALOHA simulations with experimental measurements. Spectra from the two different methods are compared in Fig. 4.7. However, for PAM the use of Langmuir probe density measurements leads to better agreement of the plasma current than the reflection coefficient matching.

It is important to be aware of the limitations of the ray-tracing/Fokker-Planck model. The spectral gap, i.e. the difference between the initial parallel refractive indices of the launched rays of the wave and the n_{\parallel} required for Landau damping, must be small enough to be bridged by toroidal refraction, which is usually the case for high temperature plasmas. For Tore Supra, this also implies low plasma density. At higher density, a regime is entered for which the validity of the ray-tracing modelling is questionable because of unrealistic ray propagation. The ray propagation can be divided into different propagation schemes that describe the trajectory of the LH ray between launching and quasi-linear absorption. The type of absorption depends on the initial parallel refractive index of the launched wave ($n_{\parallel 0}$), magnetic field strength, temperature and density profiles. The case for which the simulations are within the validity range, is the single pass absorption where the ray is absorbed without any reflections on the plasma edge or few pass absorption when the wave is absorbed in one or two reflections. In multi-pass absorption the ray propagates into the plasma but is reflected several times before reaching the absorption layer. The LH wave should be absorbed at least within a few reflections on the plasma edge, otherwise the ray propagation becomes dominated by stochasticity. Predictive LHCD simulations with the C3PO/LUKE codes have previously been performed for ITER [40]. In large, hot plasmas like the future plasmas of ITER, the LH waves can usually not reach the center, since the LH wave is strongly damped already at the edge. As a consequence of the small spectral gap, ITER-like LHCD scenarios are well described with the ray-tracing/Fokker-Planck model presented in this section.

Chapter 5

Summary

The present thesis treats aspects of lower hybrid current drive (LHCD) in the Tore Supra tokamak. Fully non-inductive operation with LHCD is achieved using either a fully active multijunction (FAM) launcher or an ITER-relevant passive active multijunction (PAM) launcher, or both launchers simultaneously. A set of codes, each describing a part in the LHCD process, are coupled in order to simulate full current drive scenarios. The modelling suite provides calculation of the electron distribution function and its moments such as the current profile and LH power deposition. A synthetic diagnostic for the fast electron bremsstrahlung (FEB) measured by the hard X-ray (HXR) cameras installed on Tore Supra is used to assess the quality of the simulations.

In [paper A](#) the full chain of modelling tools used for the LHCD simulations is presented. The reconstruction of the HXR emission from FEB diagnostic shows good agreement between simulations and fully non-inductive Tore Supra LHCD experiments with both FAM and PAM launchers in low density and high temperature conditions for which the wave power gets absorbed after few reflections on the plasma edge. In particular, the modelling has shown that the two LH launchers can produce different current profiles, even though the peak $n_{||}$ -values are the same, indicating that the details of the launched $n_{||}$ -spectrum, more precisely the negative lobes, play an important role for the current profile. Consequently, current driven by PAM results in a globally more hollow current profile than would be driven with the FAM launcher. This is a possible explanation for why LHCD with PAM and FAM give rise to different MHD behaviour in Tore Supra plasmas [12]. Another consequence is that the traditional interpretation of the Abel inverted FEB emission

profiles in the energy interval 60 – 80 keV as an estimate of the current profile, is valid for FAM type launchers but not for PAM. Because the perpendicular FEB emission does not depend on the toroidal direction of the emitting electron, the radial FEB profile is more representative of the power deposition profile than the current profile. Therefore, the PAM current profile can differ significantly from the one obtained with the FAM launcher in similar conditions, even though measurements of HXR signals due to FEB emission may be similar. For the PAM launcher, Abel inversion of the HXR profile rather gives an estimate of the LH power deposition profile.

The current drive efficiency is found to scale with the directivity according to theoretical predictions [21]. Due to the strong density dependence of the directivity, the plasma edge density is found to be a critical initial condition for the simulations. It is found that when the launcher mouth density is obtained by matching the reflection coefficient of ALOHA simulations with experimental measurements, ray-tracing and Fokker-Planck simulations provide a good estimate of the driven current. For PAM the use of Langmuir probe density measurements leads to better agreement. This contradictory result suggests that the modelling would benefit from more accurate edge density measurements and a refined modelling of the effects of the launched wave spectrum.

The model used in [paper A](#) is only valid for scenarios where the LH wave is strongly Landau damped and the parallel refractive index of the rays are absorbed after n_{\parallel} -upshift of due to toroidal refraction. The study is therefore restricted to low density or high temperature scenarios, where the gap between the nominal refractive index of the launched wave and the one required for Landau damping to take place, is small enough for the rays to be absorbed within one or few passes. Otherwise the ray propagation becomes dominated by stochasticity.

In [paper B](#) a weak LH wave damping domain is explored experimentally by LHCD in high density scenarios in Tore Supra. The central line-integrated HXR signal is found to decay strongly with density. It is concluded that the fast decay of FEB emission with plasma density could be consistent with simple scaling of the current drive efficiency. The Landau damping conditions are weak for high density and low temperature plasmas. Therefore modelling of this scenario was outside the validity frames of the current LHCD simulation tools. The toroidal upshift of the refractive index is not strong enough to bridge the spectral gap and the propagation of rays becomes dominated by stochasticity. The rays get

absorbed after many edge reflections leading to chaotic results, with indeterministic ray trajectories. This is a limitation of the simulation suite in its current state. Failed comparison of modelling with experimental results contribute to define the validity limits of the ray-tracing/Fokker-Planck model. Mechanisms responsible for bridging the spectral gap must be explored and implemented since there is experimental evidence that the wave is absorbed after few passes even in weak damping conditions where toroidal refraction is too weak to solely explain the upshift. [Paper B](#) also shows that the HXR decay with density occurs with the same slope for a wide range of plasma densities.

[Paper C](#) deals with LHCD in large spectral gap scenarios, more specifically in high density Tore Supra plasmas. The current model used in [paper A](#) is not valid for the experimental scenarios presented in [paper B](#). Still, there is experimental evidence of LH driven current from scenarios in the large aspect ratio tokamak TRIAM-1M [42] where the spectral gap must be filled even though the upshift of the parallel refractive index is almost negligible. It has been suggested that the LH wave pulls out a tail of fast electrons from the Maxwellian distribution as a seed for the quasi-linear damping [18]. In [paper C](#), the degree of spectral modification required to bridge the spectral gap is investigated. When the LH spectrum at the last closed flux surface is slightly modified with a spectral tail extension, the otherwise weakly damped wave is damped after few reflections on the plasma edge. In addition, it is shown that a fast fluctuating spectrum with respect to the electron slowing down time fills the spectral gap as well as the static one. This result suggests that the effect of density fluctuations in the scrape off layer is a good candidate for explaining LHCD in weak damping regimes.

With the new spectral tail description, the high density LHCD scenarios in [paper B](#) can be modelled. Possible mechanisms behind the modified spectra are density fluctuations in the scrape off layer (SOL) [19] or the effect of parametric decay instabilities [20]. In order to further validate the approach, the model should be tested for other tokamaks.

When the upshift due to toroidal refraction is weak, like in large aspect ratio tokamaks, it is suggested that the spectral gap is filled before the LH wave enters the plasma. Given the interesting results of [paper C](#), a next step could be to evaluate the compatibility of the possible mechanisms behind the modification of the spectrum in the SOL. The promising candidate of spectral perturbation due to edge fluctuations in the SOL [19] could eventually be implemented in the LHCD modelling

workflow.

Furthermore, the possibility of an LHCD system in ITER for current profile control could require additional predictive modelling. In these strong damping scenarios, the model used in [paper A](#) is sufficient for such calculations. The WEST configuration will provide the capability to run long pulses in the high confinement regime (H-mode), a plasma operational mode also foreseen for ITER [5]. Future LHCD experiments on WEST provide an excellent opportunity to improve understanding of LHCD physics, both from experiments and modelling in scenarios relevant for ITER, i.e. H-mode with high pedestal density and steep density gradient.

References

- [1] J. Freidberg. *Plasma Physics and Fusion Energy*. Cambridge University Press, 2007. ISBN 978-0-521-73317-5.
- [2] T. Fülöp, G. Papp, and I. Pusztai. Fusion energy lecture notes. January 2012.
- [3] JET Team. Fusion energy production from a deuterium-tritium plasma in the JET tokamak. *Nuclear Fusion*, 32(2), 1992.
- [4] *All-the-World's Tokamaks*. <http://www.tokamak.info>.
- [5] J. Bucalossi et al. The WEST project: Testing ITER divertor high heat flux component technology in a steady state tokamak environment. *Fusion Engineering and Design*, 89(7-8), 2014.
- [6] *Fusion For Energy*, January 2012. <http://fusionforenergy.europa.eu/understandingfusion/>.
- [7] S. Ejima et al. Volt-second analysis and consumption in Doublet III plasmas. *Nuclear Fusion*, 22(10), 1982.
- [8] J. Wesson. *Tokamaks*. Clarendon Press, third edition, 2004. ISBN 978-0-19-850922-6.
- [9] G.T. Hoang et al. Improved confinement in high li lower hybrid driven steady state plasmas in Tore Supra. *Nuclear Fusion*, 34(1), 1994.
- [10] X. Litaudon et al. Stationary magnetic shear reversal experiments in Tore Supra. *Plasma Physics and Controlled Fusion*, 38, 1996.
- [11] W. Horton et al. Penetration of lower hybrid current drive waves in tokamaks. *Physics of Plasmas*, 20(11), 2013.

- [12] R. Dumont et al. Multi-megawatt, gigajoule plasma operation in Tore Supra. *Plasma Physics and Controlled Fusion*, 56(7), 2014.
- [13] T. Yamamoto et al. Experimental Observation of the RF-Driven Current by the Lower-Hybrid Wave in a Tokamak. *Physical Review Letters*, 45(9), 1980.
- [14] S. Bernabei et al. Lower-Hybrid Current Drive in the PLT Tokamak. *Physical Review Letters*, 49(17), 1982.
- [15] T.H. Stix. *Waves in Plasmas*. American Institute of Physics, 1992. ISBN 0-88318-859-7.
- [16] R.A. Cairns. *Radiofrequency Heating of Plasmas*. IOP Publishing, 1991. ISBN 0-7503-0034-5.
- [17] G.M Wallace et al. Absorption of lower hybrid waves in the scrape off layer of a diverted tokamak. *Physics of Plasmas*, 17(8), 2010.
- [18] H. Takahashi. The generalized accessibility and spectral gap of lower hybrid waves in tokamaks. *Physics of Plasmas*, 1(7), 1994.
- [19] M. Madi et al. Effect of density fluctuations in the scrape-off layer on the lower hybrid power spectrum. *41st EPS Conference on Plasma Physics*, P1.046, 2014.
- [20] R. Cesario et al. Modelling of a lower-hybrid current drive by including spectral broadening induced by parametric instability in tokamak plasmas. *Physical Review Letters*, 92(17), 2004.
- [21] N.J. Fisch. Theory of current drive in plasmas. *Reviews of Modern Physics*, 59(1), 1987.
- [22] A. Ekedahl et al. Validation of the ITER-relevant Passive-Active-Multijunction LHCD launcher on long pulses in Tore Supra. *Nuclear Fusion*, 50(11), 2010.
- [23] *Landau damping*, *Wikipedia*, March 2012. http://en.wikipedia.org/wiki/File:Maxwell_dist_ress_partic_landau.svg.
- [24] D. Moreau and I. Voitsekhovitch. Plasma control issues for an advanced steady state tokamak reactor. *Nuclear Fusion*, 39(5), 1999.
- [25] G. T. Hoang et al. A lower hybrid current drive system for ITER. *Nuclear Fusion*, 49(7), 2009.

-
- [26] D. van Houtte et al. Recent fully non-inductive operation results in Tore Supra with 6 min, 1 GJ plasma discharges. *Nuclear Fusion*, 44(5), 2004.
- [27] T. Mutoh et al. Steady-state operation and high energy particle production of MeV energy in the Large Helical Device. *Nuclear Fusion*, 47(9), 2007.
- [28] J.F. Artaud et al. The CRONOS suite of codes for integrated tokamak modelling. *Nuclear Fusion*, 50(4), 2010.
- [29] J. Hillairet, D. Voyer, A. Ekedahl, M. Goniche, M. Kazda, O. Meneghini, D. Milanesio, and M. Preynas. ALOHA: an Advanced Lower Hybrid Antenna coupling code. *Nuclear Fusion*, 50(12), 2010.
- [30] Y. Peysson, J. Decker, and L. Morini. A versatile ray-tracing code for studying RF wave propagation in toroidal magnetized plasmas. *Plasma Physics and Controlled Fusion*, 54(4), 2012.
- [31] Y. Peysson and J. Decker. Calculation of RF current drive in tokamaks. CEA/IRFM, Association Euratom-CEA, 2007.
- [32] Y. Peysson and J. Decker. Fast electron bremsstrahlung in axisymmetric magnetic configuration. *Physics of Plasmas*, 15(9), 2008.
- [33] C. Gil. Diagnostic systems on Tore Supra. *Fusion Science and Technology*, 56(3), 2009.
- [34] P. Bibet, X. Litaudon, and D. Moreau. Conceptual study of a reflector waveguide array for launching lower hybrid waves in reactor grade plasmas. *Nuclear Fusion*, 35(10), 1995.
- [35] D. Guilhem et al. Manufacturing process and tests of a lower hybrid passive active multi-junction launcher for long pulse experiments on Tore-Supra. *Fusion Engineering and Design*, 86(4-5), 2011.
- [36] A. Ekedahl et al. Lower Hybrid Current Drive in Tore Supra. *Fusion Science and Technology*, 56(3), 2009.
- [37] M. Preynas et al. Coupling characteristics of the ITER-relevant lower hybrid antenna in Tore Supra: experiments and modelling. *Nuclear Fusion*, 51(2), 2011.

- [38] G.V. Pereverzev. Use of the multidimensional WKB method to describe propagation of lower hybrid waves in tokamak plasma. *Nuclear Fusion*, 32(9), 1992.
- [39] O. Meneghini, S. Shiraiwa, and R. Parker. Full wave simulation of lower hybrid waves in maxwellian plasma based on the finite element method. *Physics of Plasmas*, 16(9), 2009.
- [40] J. Decker et al. Calculations of lower hybrid current drive in ITER. *Nuclear Fusion*, 51(7), 2011.
- [41] Y. Peysson and F. Imbeaux. Tomography of the fast electron bremsstrahlung emission during lower hybrid current drive on tore supra. *Review of Scientific Instruments*, 70(10), 1999.
- [42] S. Moriyama et al. Ultra-long pulse operation using lower hybrid waves on the superconducting high field tokamak TRIAM-1M. *Nuclear Fusion*, 30(1), 1990.